JPhys Materials

LETTER • OPEN ACCESS

Flexible nanogap polymer light-emitting diodes fabricated via adhesion lithography (a-Lith)

JPhys Materials

OPEN ACCESS

RECEIVED
17 July 2018

REVISED
26 August 2018

ACCEPTED FOR PUBLICATION
29 August 2018

PUBLISHED
17 September 2018

LETTER

Flexible nanogap polymer light-emitting diodes fabricated via adhesion lithography (a-Lith)

Gwenhivir Wyatt-Moon[1], Dimitra G Georgiadou[1], Alina Zoladek-Lemanczyk[2], Fernando A Castro[2] and Thomas D Anthopoulos[1,3]

[1] Physics Department & Centre for Plastic Electronics, Blackett Laboratory, Imperial College London, Exhibition Road, South Kensington, London SW7 2BW, United Kingdom
[2] National Physical Laboratory, Hampton Road, Teddington, Middlesex TW11 0LW, United Kingdom
[3] King Abdullah University of Science and Technology (KAUST), Thuwal 23955-6900, Saudi Arabia

E-mail: thomas.anthopoulos@kaust.edu.sa

Keywords: organic semiconductors, light-emitting diode, flexible electronics, nanolithography, organic light-emitting diodes

Abstract

We report the development of coplanar green colour organic light-emitting diodes (OLEDs) based on asymmetric nanogap electrodes fabricated on different substrates including glass and plastic. Using adhesion lithography (a-Lith) we pattern Al and Au layers acting as the cathode and anode electrodes, respectively, separated by an inter-electrode distance of <15 nm with an aspect ratio of up to 10^6. Spin-coating the organic light-emitting polymer poly(9,9-dioctylfluorene-*alt*-bithiophene) (F8T2) on top of the asymmetric Al–Au nanogap electrodes results in green light-emitting nanogap OLEDs with promising operating characteristics. We show that the scaling of the OLED's width from 4 to 200 mm can substantially improve the light output of the device without any adverse effects on the manufacturing yield. Furthermore, it is found that the light-emitting properties in the nanogap area differ from the bulk organic film, an effect attributed to confinement of the conjugated polymer chains in the nanogap channel. These results render a-Lith particularly attractive for low cost facile fabrication of nanoscale light-emitting sources and arrays on different substrates of arbitrary size.

Nanometer-sized polymer light-emitting diodes (n-PLEDs) have been proposed as light sources in sub-wavelength scanning near-field optical microscopes as well as in nanoscale photo-patterning to create simultaneously a large number of identical patterns [1, 2]. Their unique advantages are colour tunability, versatility in geometrical pattern selection and ease of manufacturing of nanostructured arrays using low cost solution processing on substrates of arbitrary size and shape [3]. From an operational standpoint, miniaturised light-emitting diodes are advantageous to larger area ones, as higher current densities can be sustained thanks to efficient dissipation of Joule heating [4, 5]. Indeed a suppression of organic light-emitting diodes (OLEDs) roll-off characteristics has been observed upon narrowing the current injection/transport area down to 50 nm [6]. These developments led to demonstration of low threshold amplified spontaneous emission in light-emitting polymer films [7], which could pave the way to the realisation of electrically pumped organic lasers [8]. Further progress has, however, been hindered by manufacturing challenges, as shadow masking and conventional photolithography cannot produce nanometer-sized electrode feature between different metals, and e-beam lithography is not suitable for upscale while it is often limited to a single electrode material. We have recently introduced adhesion lithography (a-Lith) technique as a viable alternative for the scalable sub-15 nm patterning of asymmetric, i.e. of different work function, coplanar metal electrodes on large area flexible substrates [9]. The asymmetric nature of the electrodes, which is difficult to obtain with other common nanopatterning techniques, allows for a range of electronic nanogap devices to be created via simply depositing a single layer of active material on top of different combinations of electrode pairs using low temperature and inexpensive printing techniques. Successful demonstration of printed radiofrequency diodes [10–12], memory devices [13], field-effect transistors [14, 15] and ultraviolet (UV) photodetectors [16] enabled by a-Lith have been so far

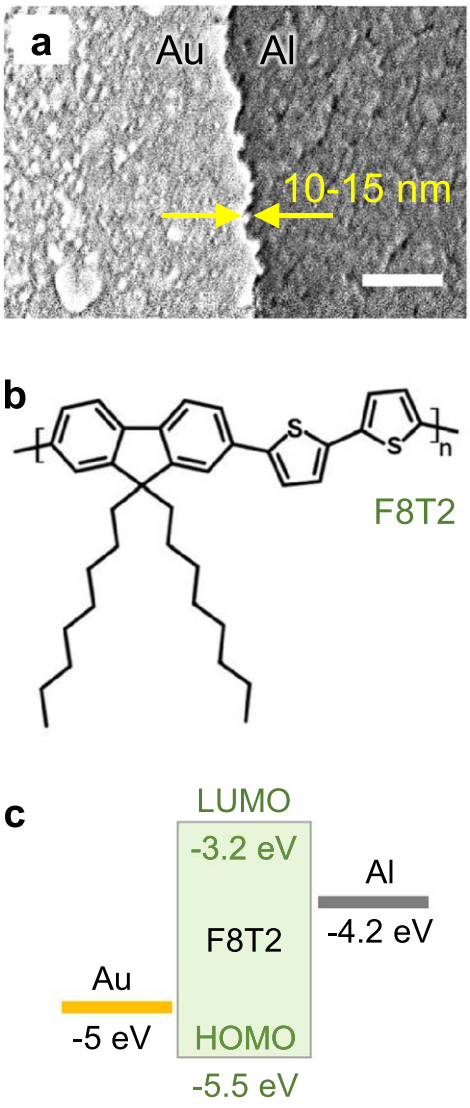

Figure 1. (a) SEM micrograph of an empty Al–Au nanogap. Scale bar: 200 nm. (b) Chemical structure of the light-emitting organic polymer poly(9,9-dioctylfluorene-alt-bithiophene) (F8T2). (c) Energy level diagram of the single layer nanogap PLED device.

demonstrated. Recently a *proof-of-concept* nanogap n-PLEDs based on four different solution-processed organic polymers, covering emission across the whole visible spectrum, has also been reported [17].

Herein we report on a-Lith fabricated coplanar green-emitting n-PLEDs on both glass and plastic substrates and study their optoelectronic characteristics. The a-Lith process steps to obtain nanogap separated asymmetric metal contacts, comprising a gold (Au) anode and an aluminium (Al) cathode, have been reported elsewhere [9, 17]. The scanning electron micrograph (recorded with a LEO Gemini 1525 field emission scanning electron microscope with the operating voltage at 5 kV) shown in figure 1(a) depicts a separation of ~15 nm between the Au and Al electrodes. To create n-PLEDs, first the as-fabricated a-Lith electrodes were placed in a UV-ozone chamber for 30 min and then the light-emitting polymer poly(9,9-dioctylfluorene-*alt*-bithiophene) (F8T2), dissolved in tetrahydrofurane (10 mg ml^{-1}), was spin-coated at 2000 rpm. The substrates were annealed at 70 °C for 10 min in a dry nitrogen glovebox to evaporate the remaining solvent. The chemical structure of F8T2 polymer is shown in figure 1(b). The latter was selected owing to its good charge transport as well as light-emitting properties [18]. All current–voltage characteristics were performed in a N_2 atmosphere using an Agilent B2902A source/measure unit, while a Si photodiode, PD, (Hamamatsu S1133) was placed vertically above the n-PLED to capture the emitted light and compare the light output when using different sized electrodes. A GXM-XJL 201A microscope with GXCAM-3 High-Resolution Digital Microscope Camera attached to the eye piece was used to record the microphotographs of the light-emitting nanogap PLEDs.

The energy level diagram of the single layer n-PLED in figure 1(c) shows that hole injection from the Au Fermi level to F8T2 highest occupied molecular orbital level is more favourable due to the lower injection barrier present at this interface (0.5 eV), as compared with the electron injection barrier at the F8T2/Al interface (1 eV).

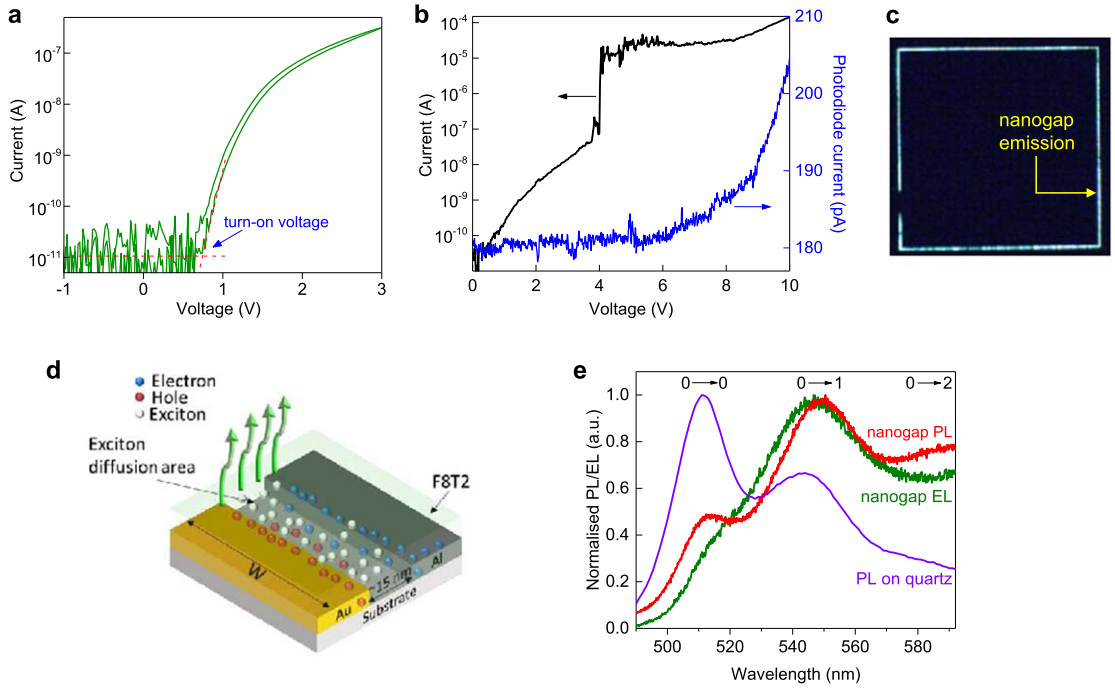

Figure 2. (a) Semi-logarithmic plot of the current–voltage characteristics depicting the diode turn-on voltage. (b) *I–V* characteristics of a F8T2 nanogap PLED and current output of the photodiode used to monitor the emitted light. (c) Optical microscope image of the PLED during operation. (d) Schematic illustration of the exciton formation in the area inside and above the coplanar Al–Au electrodes. (e) PL spectrum of F8T2 films deposited on quartz and PL and EL spectra of F8T2 n-PLEDs recorded at the nanogap region. The respective vibrational transitions assigned to each peak are also shown.

Given also the almost equal F8T2 electron and hole mobility ($\mu_{e/h,FET} \approx 5–6 \times 10^{-3}$ cm^2 V^{-1} s^{-1}) [19], holes are expected to be the majority carriers in this single-layer device structure. Indeed, the semi-log current–voltage (*I–V*) plot of the n-PLED (figure 2(a)) indicates that the nanogap diode turns on at around 0.5 V, whereas light emission occurs when the device is biased >6 V, as evidenced by the Si photodiode response in figure 2(b). Note that the exact determination of the n-PLED turn-on voltage may be limited by the specific detectivity of the photodetector used under the measurement conditions (the dark current, I_D, measured in our experimental setup was in the range of 100 pA, which is 10 times higher than the nominal $I_D = 10$ pA given by the manufacturer). The device area of 160 μm^2 (calculated from electrode height (40 nm), multiplied by its width (4 mm)) and high current allow for current densities around 875 kA m^{-2} to be calculated at 10 V which is far higher than values reported for sandwich device structures (usually 10^3–10^4 A m^{-2}) and could be of interest for organic semiconductor laser diode applications [6]. We do note, however, that this rather high current density is expected to be overestimated due to the non-ideal device geometry and the resulting current spreading over the surface of the nanogap electrodes due to the larger thickness of the organic active layer. Despite this non-ideal feature, the maximum current density within the organic layer is expected to remain significantly higher than that reported for sandwich organic devices.

Figure 2(c) shows a microphotograph of a light-emitting nanogap device, as defined by a 1 × 1 mm^2 square Au electrode surrounded by an Al electrode, when subject to 10 V bias. This geometry (given a 15 nm nanogap) would correspond to a top view emitting area of ~60 μm^2. However, light appears to be emitted from a much broader region, most likely because the resolution is limited by the microscope's optics [3, 20]. Nevertheless, we cannot disregard the fact that due to spin-coating of the polymer solution on top of the whole substrate, current flow is not entirely confined within the nanogap channel volume and may well extend beyond the active region. The 3D schematic depicted in figure 2(d) illustrates the suggested device operation and light emission mechanism. The high electric field strength induced in the nanochannel (in the order of GV m^{-1} during light emission conditions) increases the injection rate of charge carriers from the electrodes, not only in the lateral but also in the vertical direction, and thus the electron–hole recombination and exciton formation events happen at a larger volume than the one specified by the two electrodes and the nanogap channel. Higher electric fields may also promote the extension of the exciton diffusion path length and lifetime further away from the nanogap area, permitting singlet decay and light emission to occur from a wider region. Similar experimental observations as well as simulations that have been carried out with sub-micron stripe-shaped inorganic LEDs revealed a wider current spreading for higher injection currents [21]. Electrode modification of the electrodes with suitable

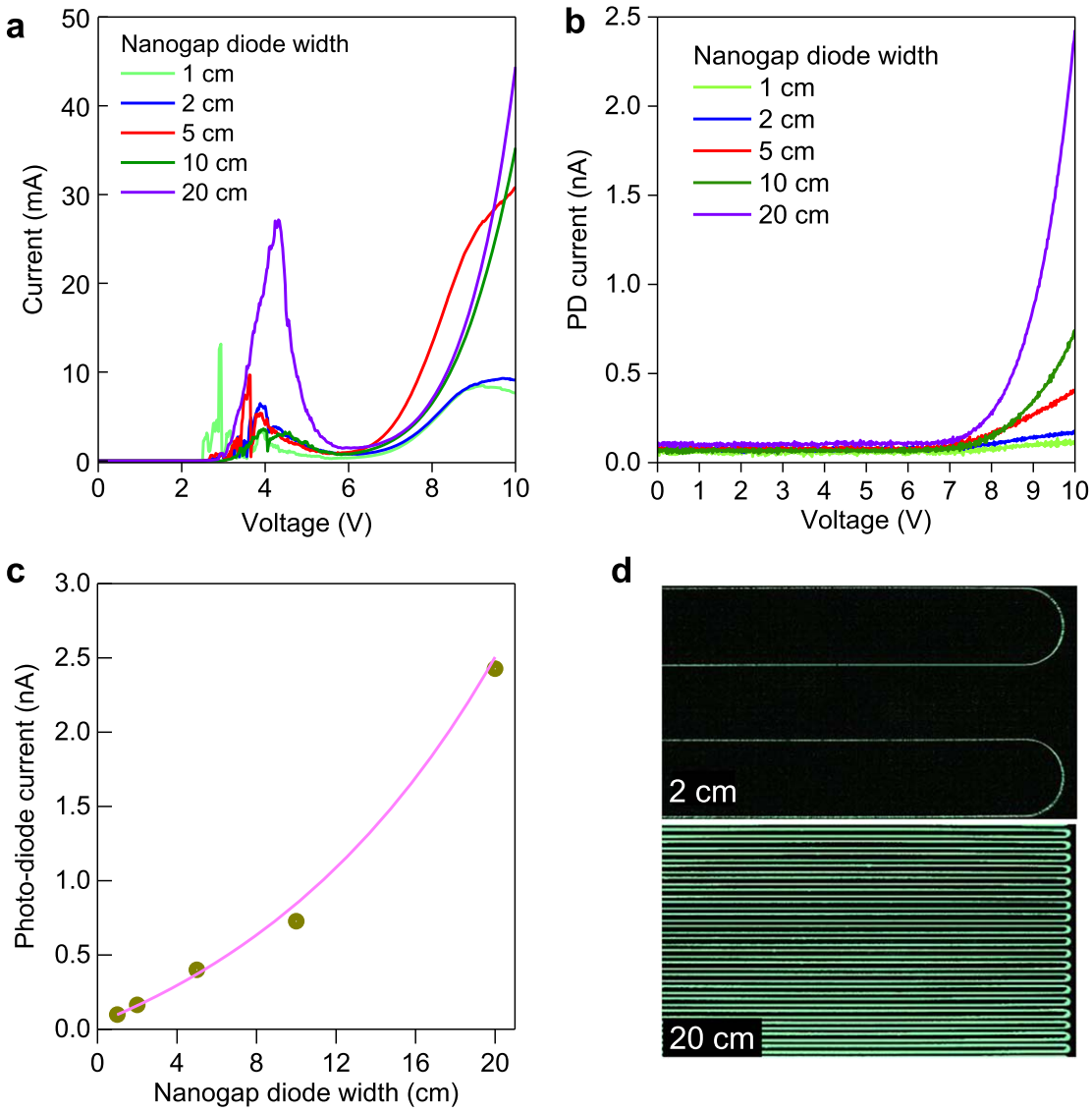

Figure 3. (a) *I–V* characteristics of n-PLEDs fabricated with different width interdigitated electrodes. (b) Photodiode response of the light emitted from the different width nano-LEDs. (c) Light output as a function of diode width fitted with a double exponential curve. (d) Optical micrographs of 2 and 20 cm width n-PLEDs under operation depicting light emission from the nanogap region.

self-assembled monolayers may provide a route towards better insulation of the electrodes and controlled emission from a narrower region.

Figure 2(e) shows the photoluminescence (PL) and electroluminescence (EL) spectra of the F8T2 thin film/nanostructured PLED device. The PL and EL spectra around the nanogap area of coplanar Au/Al electrodes were recorded using a confocal Raman PL spectroscopy system (Labram 800, Horiba France) incorporating 100x Olympus objective, 150 grooves/mm grating and The Synapse CCD detector (Horiba). The PL excitation source was 405 nm diode laser (Thorlabs). The EL spectra were recorded using the same setup upon electrically biasing the n-PLED. The PL of a reference thin film of F8T2 on quartz was recorded with a FluoroMax-3 spectrofluorimeter and it comprises a vibronic structure with a dominant peak at 511 nm, assigned to the 0–0 transition, a secondary peak at 544 nm (0–1) and a shoulder around 585 nm (0–2), in accordance with previous reports [18]. However, more interestingly, when an F8T2 film is spin-coated on top of the nanogap electrodes, these peaks appear to be red-shifted to 513, 549 and 590 nm, while the intensity of the 0–0 peak is substantially suppressed in favour of the two other peaks. These effects are likely attributed to the confinement of the polymer inside the narrow nanogap channel, acting as a template for the variation of the polymer chain orientation. More specifically, increased self-absorption in the limited space may be responsible for the shift of the highest PL intensity from the 0–0 to 0–1 vibronic transition [22], while the red shift can also be attributed to an increase of effective conjugation length due to chain planarization, favouring intrachain against interchain energy transfer. The latter would result in the higher energy excitons migrating into the lower energy states along the same chain, inducing the observed spectral red-shift [23]. The EL spectrum follows closely the shape of the nanogap derived

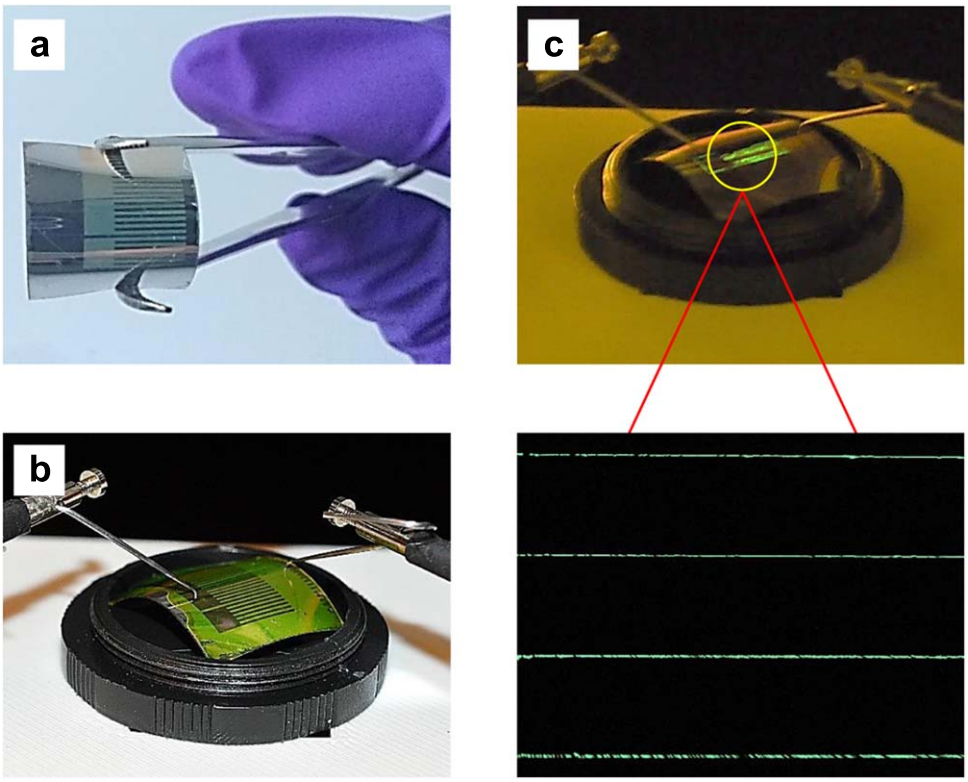

Figure 4. Photographs of the plastic nanogap PLED device. (a) a-Lith fabricated Al–Au nanogap structures on a PET substrate. (b) F8T2 light-emitting polymer spin-coated on top of the Al–Au nanogap electrodes and placed in the measurement setup. (c) Light emission from a F8T2-based nanogap PLED device during operation and under mechanical bending and a zoomed-in optical micrograph of the diode's light-emitting region.

PL, the main emission peaking at 547 nm with a shoulder at 512 and 592 nm. It should be noted here that EL is by definition emitted through the spatially constrained area of the recombination zone, whereas PL is usually an averaged emission from the whole excitation volume. The similarity between the EL and PL spectra measured at the nanogap area reveal a similar light emission mechanism dominating these structures despite the different excitation source.

As a next step, we explored ways of increasing the light output from the n-PLED device via dramatically increasing the aspect ratio of the device. The latter is defined as the ratio of the electrode width by the channel length. This was achieved simply by changing the mask design used to pattern the first metal electrode from square to an interdigitated shape with varying pitch size (distance between interdigitated fingers) to allow for diode widths ranging from 1 to 20 cm, while the electrode thickness remained constant at 40 nm. Scaling the diode width has been proven beneficial for both radiofrequency diodes [12], by further enhancing their current driving capabilities, as well as for photodetector applications [16], since it allows significant increase of the photocurrent, whilst retaining the diode's dark current at relatively low levels. Figure 3(a) shows the *I–V* characteristics of each nanogap PLED device upon increasing the electrodes size. Noteworthy is the observation of negative differential conductance in all devices between 3–6 V, a feature also present in the *I–V* characteristics of figure 2(b). Although elucidating the origin of this feature could be interesting, it is beyond the scope of this work and will be the subject of future studies. Despite this, all *I–V* characteristics show a similar shape with the current at higher biases scaling with the device width, in accordance with previous results. For instance, the current measured in the 1 cm width diode at 10 V (7.6 mA) is over an order of magnitude larger as compared to the 4 mm width device (0.14 mA) shown in figure 2(a). To give an estimate of the range of current densities obtained with our devices, we have used the geometrical area of various electrode widths and calculated current densities (the geometrical area calculation is mentioned above and also reported in our recent publication [17]) ranging from circa 5×10^5 to 2.5×10^6 mA cm^{-2} for the interdigitated 20 and 1 cm-long electrodes, respectively, shown in figure 3(a). These values are in accordance with other nanoscale OLED reports containing devices of similar active area, although based on a vertical architecture [24].

Interestingly, the current measured by the Si photodiode, corresponding to the intensity of the light emitted by these device (figure 3(b)), increases exponentially with the diode's width (i.e. the perimeter of the interdigitated electrodes), while the nanogap channel length (i.e. the inter-electrode distance) remains constant

in all cases at ~15 nm (figure 3(c)), validating our initial hypothesis of using these high aspect ratio coplanar diodes to obtain higher luminance. Figure 3(d) depicts two characteristic optical micrographs of a 2 cm and a 20 cm device during operation, clearly showing this increase in brightness per substrate unit area.

Finally, we were able to demonstrate n-PLED devices fabricated on plastic flexible substrates. More specifically, the a-Lith procedure was carried out on polyethylene terephthalate (PET) films (Dupont) in the same manner as on the glass substrates. Figure 4(a) shows the as-prepared a-Lith Al–Au electrodes patterned on PET. Here, the interdigitated Au fingers are serving as the anode and are surrounded by a common (global) Al cathode electrode. Figure 4(b) shows the flexible F8T2-based n-PLED device in our measurement setup. The *I–V* and light emission properties were very similar to the ones described above, with light emission occurring between 6.5–10 V. The optical micrograph of the light-emitting device taken during biasing at 10 V is shown in figure 4(c). The bending of the substrate was on the macro scale and appears to have had little effect on the nanoscale devices performance as light emission could be still observed under substrate stress. To the best of our knowledge this is the first example of a flexible nano-PLED fabricated on a plastic substrate. The consistency of these results with the ones obtained on glass substrates demonstrate the versatility of a-Lith to create large size nanogap devices on a variety of substrate materials.

In summary, we employed adhesion lithography to demonstrate single layer nanoscale PLEDs based on the green-emitting polymer F8T2, fabricated with coplanar asymmetric nanogap electrodes on glass and PET substrates. Despite the active area being constrained within the <15 nm nanogap channel, the large aspect ratio ($>10^6$) of the electrodes attained upon increasing the width of device from 0.4 to 20 cm allowed for higher brightness levels. These results pave the way to the high throughput and low cost fabrication of nanoscale light sources and arrays thereof. Furthermore, these coplanar structures are ideal test beds for novel light-emitting nanomaterials, such as quantum dots [25] and 2D materials [26], which usually require coplanar rather than vertical electrodes. Finally, better understanding of the operation mechanism will enable optimisation of the PLED performance to satisfy the requirements posed by the respective application.

Acknowledgments

This work was supported by the European Union's Horizon 2020 research and innovation programme (under the Marie Skłodowska-Curie grant agreement 706707) and the Engineering and Physical Sciences Research Council (EPSRC) grant no. EP/G037515/1.

ORCID iDs

Gwenhivir Wyatt-Moon https://orcid.org/0000-0002-0694-5297
Dimitra G Georgiadou https://orcid.org/0000-0002-2620-3346
Thomas D Anthopoulos https://orcid.org/0000-0002-0978-8813

References

[1] Granstrom M, Berggren M and Inganas O 1995 Micrometer-sized and nanometer-sized polymeric light-emitting diodes *Science* **267** 1479–81
[2] Iyengar N A, Harrison B, Duran R S, Schanze K S and Reynolds J R 2003 Morphology evolution in nanoscale light-emitting domains in MEH-PPV/PMMA blends *Macromolecules* **36** 8978–85
[3] Yamamoto H *et al* 2005 Nanoscale organic light-emitting diodes *Nano Lett.* **5** 2485–8
[4] Boroumand F A, Hammiche A, Hill G and Lidzey D G 2004 Characterizing Joule heating in polymer light-emitting diodes using a scanning thermal microscope *Adv. Mater.* **16** 252–6
[5] Matsushima T, Sasabe H and Adachi C 2006 Carrier injection and transport characteristics of copper phthalocyanine thin films under low to extremely high current densities *Appl. Phys. Lett.* **88** 33508
[6] Hayashi K *et al* 2015 Suppression of roll-off characteristics of organic light-emitting diodes by narrowing current injection/transport area to 50 nm *Appl. Phys. Lett.* **106** 93301
[7] Kim D H *et al* 2017 Extremely low amplified spontaneous emission threshold and blue electroluminescence from a spin-coated octafluorene neat film *Appl. Phys. Lett.* **110** 23303
[8] Kuehne A J C and Gather M C 2016 Organic lasers: recent developments on materials, device geometries, and fabrication techniques *Chem. Rev.* **116** 12823–64
[9] Beesley D J *et al* 2014 Sub-15 nm patterning of asymmetric metal electrodes and devices by adhesion lithography *Nat. Commun.* **5** 3933
[10] Semple J *et al* 2016 Radio frequency coplanar zno schottky nanodiodes processed from solution on plastic substrates *Small* **12** 1993–2000
[11] Semple J, Rossbauer S and Anthopoulos T D 2016 Analysis of schottky contact formation in coplanar Au/ZnO/Al nanogap radio frequency diodes processed from solution at low temperature *ACS Appl. Mater. Interfaces* **8** 23167–74
[12] Georgiadou D G, Semple J and Anthopoulos T D 2017 Adhesion lithography for fabrication of printed radio-frequency diodes *SPIE Newsroom* (doi:10.1117/2.1201611.006783)

[13] Semple J, Wyatt-Moon G, Georgiadou D G, McLachlan M A and Anthopoulos T D 2017 Semiconductor-free nonvolatile resistive switching memory devices based on metal nanogaps fabricated on flexible substrates via adhesion lithography *IEEE Trans. Electron Devices* **64** 1973–80
[14] Kawanago T and Oda S 2016 Utilizing self-assembled-monolayer-based gate dielectrics to fabricate molybdenum disulfide field-effect transistors *Appl. Phys. Lett.* **108** 041605
[15] Kawanago T, Ikoma R, Wanjing D and Oda S 2016 *2016 46th European Solid-State Device Research Conf. (ESSDERC)* pp 291–4
[16] Wyatt-Moon G, Georgiadou D G, Semple J and Anthopoulos T D 2017 Deep ultraviolet copper(I) thiocyanate (CuSCN) photodetectors based on coplanar nanogap electrodes fabricated via adhesion lithography *ACS Appl. Mater. Interfaces* **9** 41965–72
[17] Semple J *et al* 2018 Large-area plastic nanogap electronics enabled by adhesion lithography *npj Flexible Electron.* **2** 18
[18] Levermore P A, Jin R, Wang X, de Mello J C and Bradley D D C 2009 Organic light-emitting diodes based on poly(9,9-dioctylfluorene-co-bithiophene) (F8T2) *Adv. Funct. Mater.* **19** 950–7
[19] Chua L-L *et al* 2005 General observation of n-type field-effect behaviour in organic semiconductors *Nature* **434** 194–9
[20] Boroumand F A, Fry P W and Lidzey D G 2005 Nanoscale conjugated-polymer light-emitting diodes *Nano Lett.* **5** 67–71
[21] Gong Z, Guilhabert B, Chen Z and Dawson M D 2014 Direct LED writing of submicron resist patterns: towards the fabrication of individually-addressable InGaN submicron stripe-shaped LED arrays *Nano Res.* **7** 1849–60
[22] Martin J *et al* 2014 Poly(3-hexylthiophene) nanowires in porous alumina: internal structure under confinement *Soft Matter* **10** 3335–46
[23] Lee T-W, Park O O, Kim J-J, Hong J-M and Kim Y C 2001 Efficient photoluminescence and electroluminescence from environmentally stable polymer/clay nanocomposites *Chem. Mater.* **13** 2217–22
[24] Setoguchi Y and Adachi C 2010 Suppression of roll-off characteristics of electroluminescence at high current densities in organic light emitting diodes by introducing reduced carrier injection barriers *J. Appl. Phys.* **108** 064516
[25] Tripathi L N *et al* 2015 Quantum dots-nanogap metamaterials fabrication by self-assembly lithography and photoluminescence studies *Opt. Express* **23** 14937–45
[26] Kim Y D *et al* 2015 Bright visible light emission from graphene *Nat. Nanotechnol.* **10** 676–81